Coming Challenges in Electrified Transportation and Impact on Electrical Insulation Reliability: Ships and Aircrafts

Electrified-transportation assets move towards standards of performance, in terms of specific power and efficiency, which cause severe concerns about insulation systems reliability and resilience. New design procedures and new insulating materials must be developed to reach the high level of reliability, life and safety that are required. This paper proposes answers to such potential issues, discussing innovative design and validation approaches. Design of insulation systems must be based on the understanding and modelling the most harmful ageing processes and on the development of innovative partial discharge measurement technologies. Partial discharge (PD) measurements must provide clear indication of the type of source generating partial discharges, thus of their level of harmfulness, and of the insulation sub-subsystem where PD, as extrinsic accelerated aging phenomena, may cause reliability and resilience drop. The goal is to design an insulation system as PD-free, keeping a concept of reliability redundance which will enable, even in the case of PD inception, to reach a specified life and reliability. Examples of the applications to printed circuit-boards, cables and to a surface-discharge test cell at variable pressure suggest that the new design procedure proposed here can address accelerated aging and premature failure issues, and also that innovative PD monitoring tools must become a fundamental resource for diagnostics and the implementation of condition-based maintenance procedures.

Keywords: *Electrified transportation, insulation reliability, aging, partial discharge inception modelling, partial discharge-free design of insulation systems, condition-based maintenance*

Introduction

The irreversible trend of electrified transportation is to replace AC transformers with power electronics, with the purpose of improving efficiency, specific power, multifunctionality and dynamics of supply and distribution systems. An example is the hybrid grid paradigm: power converters/inverters can provide the type of supply power which could be needed, case by case, to optimize asset operation, from AC modulated to DC voltage.

On one hand, increasing specific power and efficiency means rising operating voltage, modulation frequency and temperature, besides reduce switching time, which can be achieved increasing electrical and thermal stresses in insulating materials and systems [Montanari et al. 2020, Montanari et al. 2019a].

In such conditions, insulation systems might suffer accelerated intrinsic electrothermal and extrinsic aging. This must drive new design criteria, quality and commissioning test procedures, diagnostic and condition-based maintenance approaches.

This paper illustrates some of the research activities carried out at the Center for Advanced Power Systems (CAPS) of Florida State University, focusing on innovative, reliable design of insulation systems for ship, aircraft and aerospace infrastructures. Reliability can be achieved innovating the concept of equipment design and operation. As regards the former, an insulation system must be designed as free from extrinsic aging (e.g. partial discharge (PD) free), and using a reliability redundance concept (besides being free from extrinsic aging, materials that can withstand such aging, if and when occurring, should be used). For the latter, condition monitoring systems, fully automatic and unsupervised, must be developed to guarantee prompt information about potential failure risks. The innovative three-leg approach has been proposed for an extrinsic-aging free insulation design, which are reviewed in Section 2, and a new automatic software is being developed to detect and monitor PD, as well as achieve straightforward information about electric asset component condition (dynamic health index). Examples of PD detection at atmospheric and reduced pressure, using the automatic, unsupervised approach, are shown in the last Section, referring to both test objects able to simulate typical defects triggering PD, and full-size insulation systems (as cables and printed circuit-boards).

Partial-Discharge Free Design and Reliability Redundancy

Recently, the innovative "three-leg" approach to insulation system design has been introduced for critical electrified transportation applications, where e.g., modulated AC voltage and hybrid supply may be involved, [Nath et al. 2023, Yang et al. 2023].

It is based on three steps (legs): 1- electric field (and thermal stress) simulation, 2- extrinsic aging threshold modelling (partial discharge inception field and voltage in combination with leg 1), 3- PD measurements for validation of the first two legs.

If an insulation system design relies upon laws governed by intrinsic aging models, such as the inverse power model for electrical life or the Arrhenius model for thermal life, [Montanari et al. 2022a], once design stresses are determined, long-term reliability (often, even if improperly, called resilience) can be achieved. However, extrinsic aging, such as that caused by partial discharges, can be occurring under operation, due to, e.g., improper manufacturing of the insulation system, stresses larger than those accounted at the design stage, aging effects. A PD-free design can be nevertheless reached, knowing models for bulk and surface PD inception, so that the risk of PD can be avoided or at least minimized (for example, taking into account the presence of internal effects up to a given size [Ramin et al. 2021]). However, while aging effects can be theoretically handled by such PD-free design, in practice it is not easy to account for real stresses under operation, their effect on insulation system integrity and, in addition, the extent of stresses that can occur changing scope of mission, electrical asset structure, loading and type of voltage waveform (as an example, supplying an asset component, such as a cable, under DC instead of AC as planned at design stage

[Montanari et al. 2019b], or not considering properly the effect of pressure, such as in electrical aircraft component design).

Here the further concept of reliability redundancy can help. Even if the effect of aging (especially thermo-mechanical) can create defects that may incept PD during operation time, and/or factors of influence, such as pressure, can change drastically the partial discharge inception voltage level, [Lusuardi et al. 2019] (and incept PD only when e.g. an aircraft is at its cruise altitude, or an electrical asset PD-free on earth is, e.g., deployed on Mars), the specified reliability will not be affected because PD-resistant materials are used for the design and manufacturing of the insulation system.

PD Free Design: Three Leg Approach

1st Leg: Electrical Field Simulation

FEM software (as COMSOL) can be used to calculate field distribution in an insulation system. Both bulk and surface insulation sub-components must be considered, and the field profile from HV conductive parts to ground obtained. Figures 1 and 2 show examples of field distribution and profile in the bulk and on the surface of a PCB supplied at 5 kV [Yang et al. 2023]. This will allow the maximum electrical stress which is the reference for insulation design (thickness, Fig. 1, and surface clearance, Fig. 2), to be determined, upon having the availability of the models described in the next section. It is noteworthy that environmental pressure does not influence this leg.

Figure 1. *Relation between the mean bulk electric field between the two copper plates of a PCB and insulation thickness. (supply voltage 5 kV).*

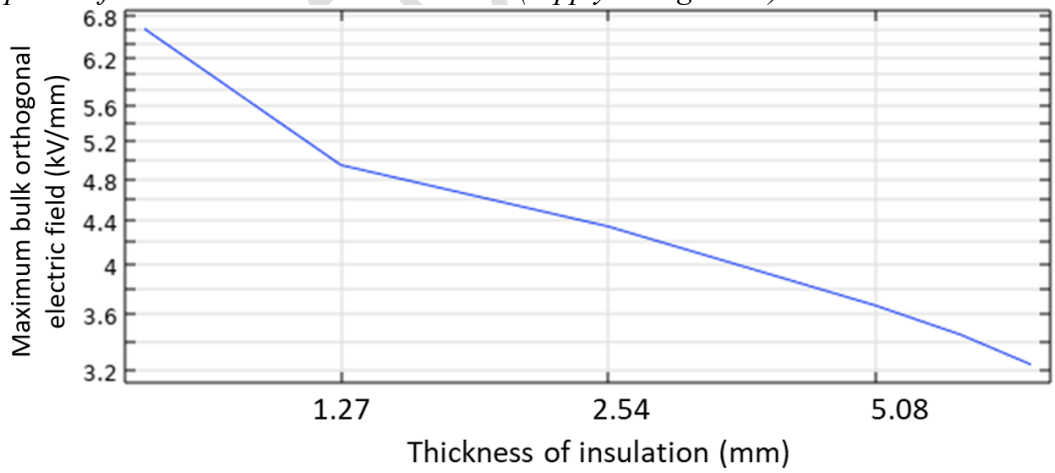

Figure 2. *Electric field profiles as a function of the distance between HV connector and ground plane in the PCB of Fig. 1 (supply voltage 5 kV).*

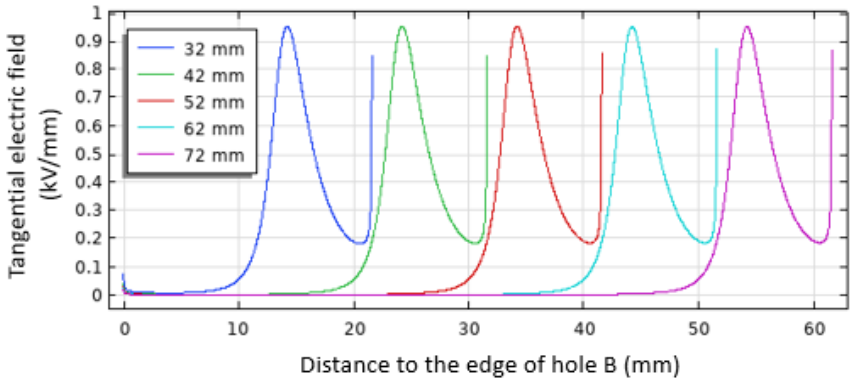

2nd Leg: Modeling

Modelling encompasses life, PD in bulk defects and PD on the surface. The most common life model to determine design field of insulation systems is based on the inverse power law [Montanari et al. 2019b]:

$$L = t_R \left(\frac{E}{E_R}\right)^{-n} \frac{f_0}{f} \qquad (1)$$

where L is life, E electrical stress, E_R is reference electric stress (generally close to the electric strength), t_R is failure time at applied field $E = E_R$, n is voltage endurance coefficient, f_0 is the reference frequency (e.g., 50 or 60 Hz) and f the AC sinusoidal frequency or modulation/carrier frequency (depending on inverter level number) for AC modulated. Note that the quantities in model (1) depend on temperature, making (1), as a matter of fact, an electrothermal life model. Also note that for DC electrical aging (1) still holds, referring to the maximum voltage (field), and n is generally larger than for AC aging (this accounting for the larger extent of stress provided by AC compared to DC, even for the same value of E).

The design field, E=E_D, can be estimated from equation (1) once the design life, L_D, is specified, $L = L_D$, and a failure probability is chosen. Upon application of (1), the maximum design field can be established, and knowing the field distribution and the nominal maximum voltage, the insulation thickness can be determined. The criterion is that the maximum field must be lower or equal to the maximum design field (at the detected failure probability and for the specified life).

The partial discharge inception field can be estimated resorting to an approximate, deterministic model derived from [Niemeyer et al. 1995, Cambareri et al. 2022]:

$$E_i = \left(\frac{E}{p}\right)_{cr} \cdot p\left(1 + \frac{B}{(pk_s l)^{\frac{1}{\beta_i}}}\right) \qquad (2)$$

where E_i is PD inception electric field, p is pressure, l is distance between positive and negative electrodes or internal defect height, B and β_i are parameters related to the physics of the ionization process [Niemeyer et al. 1995], k_s is a scale factor taking into account the field gradient, i.e. the shape of field profile [Cambareri et

al. 2022]. The value of k_s ranges from 1 when the field is uniform (thus providing the model for internal defects as in [Niemeyer et al. 1995]) to very low values when the field is strongly divergent, as in Fig. 2. Expressions for k_s are provided in [Cambareri et al. 2022].

Model (2) will take into account the risk of PD inception in bulk defects and on insulation surface, thus exploiting the PD-free design concept. Specifically, varying the voltage in the 1st leg simulations, the level of voltage at which the maximum field in insulation system bulk or surface exceeds (2) is the partial discharge inception voltage (PDIV). PDIV must be higher than then nominal voltage to have a PD-free design.

The availability of analytical PD inception model can also enable calculation of the maximum size of defects (cavities) allowed in the bulk or the minimum distance between HV and ground (creepage) on surfaces. Figure 3 reports an example of bulk insulation design, where the specified life is provided by design field ≤ 5 kV/mm, but there is a cavity able to incept PD if the field inside becomes larger than the criterion provided by eq. (2). As can be seen, there are three cases: (a) design unfeasible since both life is shorter and PD can incept, case (b) which also does not provide satisfactory design because the field in the cavity cannot incept PD, but the maximum field in the bulk is > 5 kV/mm (thus shorter than specified life) and, finally, case (c) that gives full feasibility.

It is noteworthy that eq. (2) displays and explicit dependence on pressure, which makes this leg sensitive to the level of altitude at which PD can be activated and to the PD phenomenology itself [Lusuardi et al. 2019].

Figure 3. *Electric field in insulation bulk and in an oblate delamination with height h=20 μm (l in eq. (2)) for three values of insulation thickness. Design field ≤5 kV/mm, nominal voltage 5 kV. (a) Insulation thickness d_1 =0.7 mm, mean field in insulation=7.1 kV/mm, field in the cavity= 17.8 kV/mm (almost coincident to the PD inception field in the cavity, i.e., 18.0 kV/mm, eq. (2)): design unfeasible. (b) Insulation thickness d_2 = 0.9 mm, mean field in insulation > 5.5 kV/mm, field in the cavity=13.9 kV/mm, thus design without PD, but insulation with shorter-than-design life. (c) Insulation thickness d_3 = 1.1 mm, mean field in insulation < 5 kV/mm, field in the cavity=11.3 kV/mm, thus feasible design*

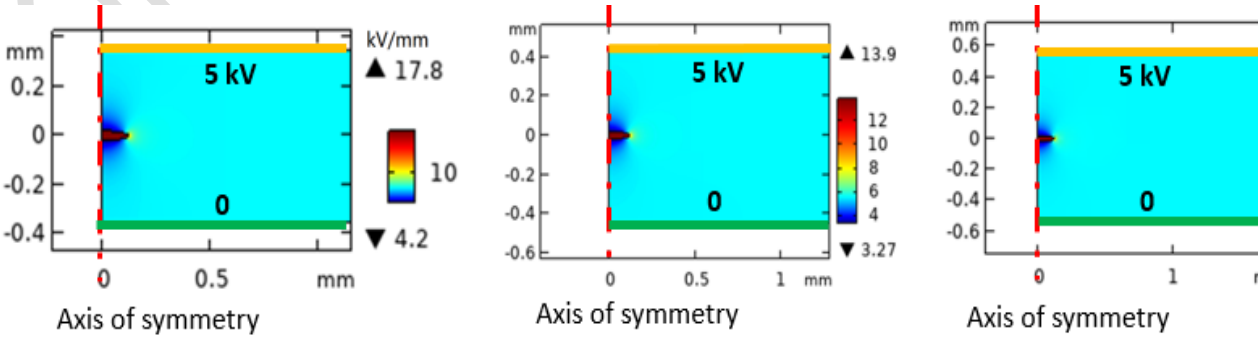

(a) (b) (c)

3rd Leg: PDIV Measurements

As mentioned above, the measurement of PDIV (which is a stochastic quantity) for a given supply voltage waveform is a fundamental tool for design and for the validation of 1st and 2nd leg.

However, PD measurements can fit to the three-leg approach at best if the technology for measuring PD is able to identify the type of defect generating PD, i.e., whether internal or surface [Contin et al. 2002]. An innovative algorithm for PD measurements and monitoring which fits to the above requirement is described in [Montanari et al. 2022b]. It is able to automatically separate and recognize noise and PD, and to identify the source generating PD (separation is carried out through Principal Component Analysis (PCA), recognition by statistical tests based on acquired signal shape, while identification relies upon artificial intelligence technique, precisely Fuzzy logic, applied to sub-patters obtained from separation). Identification is of utmost importance in the insulation system analysis, because any design or remedy action that can be taken based on PD assessment has to be driven by the type of PD, namely whether generated by internal defects or occurring on the insulation surface (generally starting from triple points where electrode edge, insulation surface and air interact).

Figure 4. *PD measurements carried out by the innovative technology: (a) Global pattern (b) Example of PD pulse waveform (c) Separation (PCA map) with clustering (d) PD Sub patterns (e) Recognition of noise and PD and Identification with likelihood of 86% surface, and 14% internal*

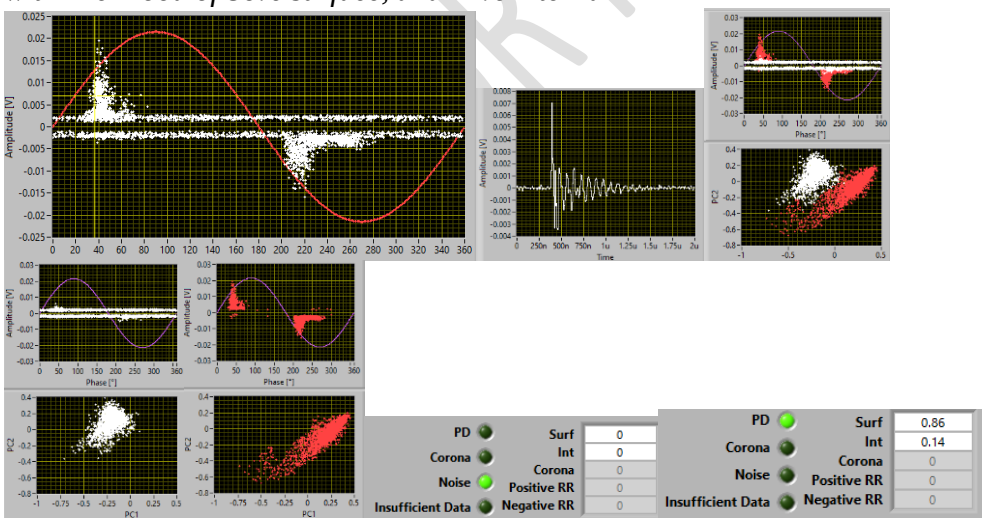

Figure 4 shows an example of PD measurement according to such innovative approach. The figure reports a case of measurements at 1.1 PDIV, with two sub-clusters in the PCA map, one recognized as noise and one as PD, and identification with likelihood of PD typology 86% surface, 14% internal. The likelihood derives from the use of fuzzy logic to implement automatically the identification step. Fuzzy logic mimics human expert approach, which is based on rules based on experience and PD physics, thus in some cases high level of uncertainty may be achieved even in expert evaluation. All the measurement and

analytics process is automatic and unsupervised. As a note, this leg is broadly influenced by environmental pressure in terms of PD pattern, PD pulse shape, detection bandwidth. The latter must be large (up to tens of MHz), but also with lower cut frequencies in the kHz range. The expectation is that by the decreasing pressure, PDIV decreases, too, and PD magnitude increases, even if contrasting indication are provided in literature [Lusuardi et al. 2019, Rui et al. 2010]. Anyway, PD testing methodology and the analytics described above would not change with pressure.

Reliability Redundance: Optimized Design

Back to reliability redundancy, there is another feature that this concept can support, that is, optimized design. Functional constraints (amount of specific power, limited space, bad heat dissipation, etc.) can make a PD-free design difficult to be reached. The concept behind is still to use insulating materials that can withstand extrinsic aging, permanent or discontinuous (as in an aircraft taking off and landing), such as corona (or PD) resistant materials. In this way, even if a "moderate" level of PD is triggered (permanently or periodically/occasionally) the design life at a selected failure probability can be still achieved because the design life and stresses have been related to the long-term performance of PD-resistant materials (under continuous PD aging). Hence, the reliability redundancy approach can be also used to obtain an optimized design when the PD-free concept cannot be applied for various reasons (e.g., due to allowed surface or volume dimensions, amount of stress, problematic heat dissipation). PD may be incepted, but the use of PD-resistant materials will nevertheless provide the specified life. Figure 5 shows an example of design made according to eq. (1) (inverse power model) which highlights that the design life is reached, even when PD are active, using a PD-resistant material, and if PD are either absent or intermittent life is longer than the design one (extra-life= L'_D-L_D).

Figure 5. *Life-lines according to the inverse power model for a PD resistant material affected or not by PD during life. E_D and L_D are specified design maximum field and life, L'_D is life at the design field for a PD-resistant material when PD are not active (thus providing higher voltage endurance coefficient and longer life)*

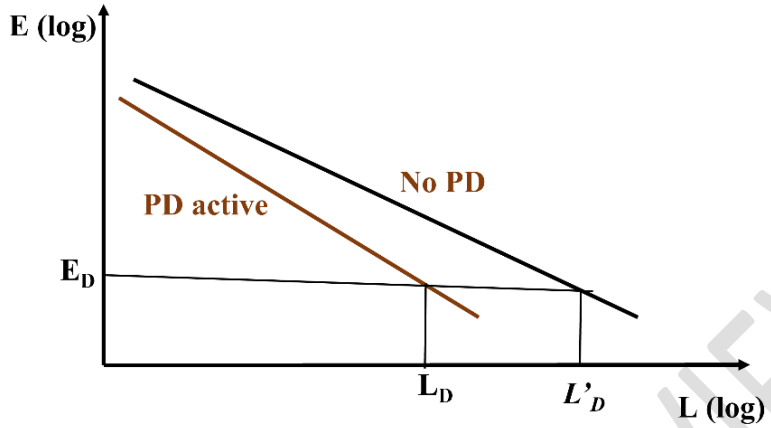

Application Examples

Application examples are relevant, here, to MV printed circuit-boards and MV cables. A further case is considered, where the criticality of surface insulation design for and transportation means used at variable pressure, lower than atmospheric, is highlighted.

PCB, Bulk, and Surface Insulation Design

There is consolidated experience in design of printed circuit-boards, PCB, for power electronics applications in LV, but very little in the MV range, especially in avionics. In MV electric field can be large for both bulk and surface insulation, with the risk of shorter-than-specified life, as well as risk of internal and surface PD. Figure 6 summarizes the first leg of a PD-free design, i.e. 2D electric field simulation for a proposed PCB design (nominal voltage V_N= 5 kV), that should fit to the 2nd leg constraints for specified life and PDIV (surface and internal) < V_N, see Figs. 1-3 [Yang et al. 2023]. The mean bulk field is around 2.5 kV/mm which is well lower than the design field, i.e., 5 kV/mm at failure probability 1%, as derived by accelerated life tests (thus the failure time at probability 1% should be much larger than the design life, in the absence of internal cavities able to incept PD). The maximum surface PD inception field is also quite limited (0.95 kV/mm), see Fig. 2. On the other hand, model (2) with k_s expressed by, [Cambareri et al. 2022]:

$$k_s = (l(0.95E_M)^+ - l(0.95E_M)^-)/l \qquad (3)$$

(where superscripts + and – indicate the field profile curve derivative and E_M is the maximum or peak field, see Fig. 2) provides an inception field for surface PD (eq.

(2)) E_{is} = 1.2 kV/mm, which is higher than the maximum tangential field as obtained from simulations and corresponds to estimated PDIV of about 6 kV. Considering the nominal voltage of 5 kV, the expectation is that PD should not incept at the standard operation voltage and atmospheric pressure.

This was confirmed by PDIV measurements: the PDIV mean value is 5.6 kV which corresponds to maximum (peak) surface tangential field (based on the 2D simulation carried out under the 1st leg) of 1.16 kV/mm, i.e., very close to model estimates. An example of PD acquisition at 1.3 PDIV is reported in Fig. 7. It shows the global PRPD pattern and the sub-patterns obtained after separation, as well as automatic recognition of noise and identification of PD. It can be seen, the PD source is identified as certainly of surface typology (likelihood 1), which highlights that measured PD are, as requested by modelling, of surface nature and they can, therefore, help in surface insulation design (and diagnostics).

Figure 6. *2D Electric field modelling. Above: field distribution, maximum and mean bulk electric field modulus, below field distribution and profile of tangential electric field*

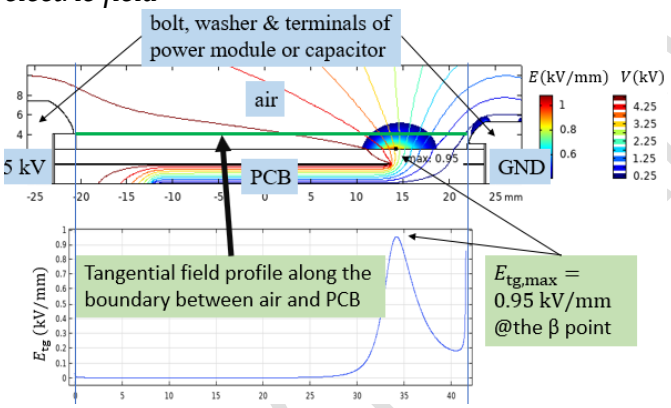

Figure 7. *Example of PD acquisition on a PCB at 1.3 PDIV using an innovative automatic PD system. (a) Global PRPD pattern (b) Separation (PCA) map with two clusters (c) Sub-patterns corresponding to each cluster of (b) (d) Recognition and identification of the type of PD source (internal, surface, corona). The likelihood of each identification is reported (surface with likelihood 1).*

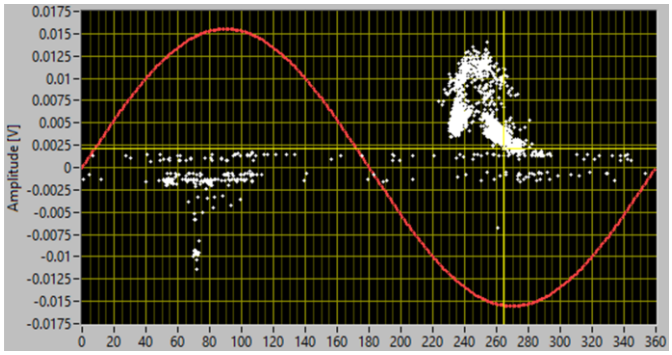

(a)

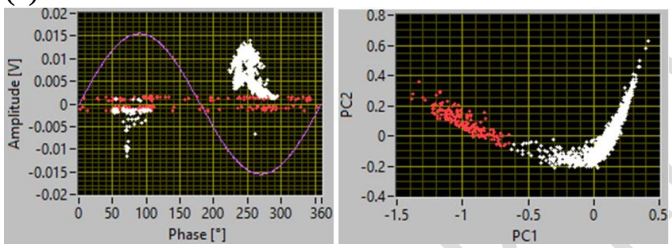

(b)

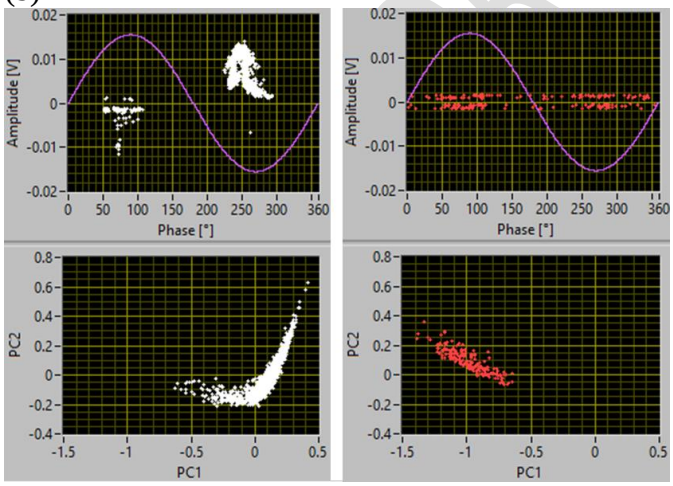

(c)

(d)

An interesting observation comes from Fig. 2: when calculating the maximum tangential field as a function of the distance between PCB contacts (high voltage to ground), the maximum field value does not change significantly.

This indicates that in the presence of significant field gradients, the distance to ground connector (creepage) may not influence noticeably the PD inception field (hence attention should likely be devoted on connector-copper strip shape rather than increasing creepage). Thus, it is the risk of surface PD inception which has to drive the design rather than the creepage length: while the latter would prevent from macroscopic discharges, the former is associated with the inception of a mechanism causing accelerated extrinsic aging and premature failure. Also, this highlights that it might happen that a fully PD-free design is not feasible, thus the concept of reliability redundancy would have to be exploited.

Cables, Surface Insulation Design

This example has the purpose to show the three-leg approach application for surface insulation design in cables.

The test arrangement is depicted in Fig. 8, having the purpose to simulate surface defects able to generate PD, as at cable terminations or splices. The high voltage (HV) electrode is constituted by the central copper conductor, which is energized from the other side of the cable (not shown in the figure). The ground (GND) electrode is realized by wrapping two foils of aluminum tape on the external jacket of the cable, at a fixed distance from the edge (clearance, segment BC in Fig. 8). Each foil is folded once to allow for field control at the triple point between aluminum, external jacket and air (point C in Fig. 8). The foils are then connected to the actual ground through another wire (visible at the top right corner of Fig. 8). The field profile varying BC distance is displayed in Fig. 9. As can be seen, electric field is highly divergent (as planned) and, as for PCB, increasing distance the maximum (peak) field has relatively small decrease. An example of automatic PD measurement, at 1.1 PDIV is shown in Fig. 10. The identification is surface PD with 100% likelihood, as expected for the created defect.

Figure 8. *Model MV cable used for the application of the three-leg approach. The cable is constituted by a copper central conductor, one EPR insulation layer (gray) and one external CPE jacket layer (black). The rated voltage of the cable is 2 kV. Path ABC represents the creepage line*

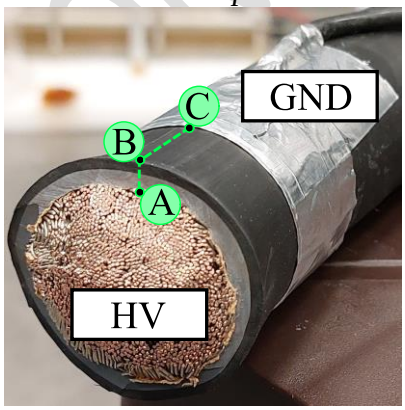

The outcome of 1st, 2nd and 3rd legs are summarized in Table 1, where maximum (peak) field, E_{sp}, PD inception fields, E_i (eqns. (2), (3)), PDIV calculated from legs 1 and 2, *PDIVe*, and the measured value, *PDIVm*, are reported. It can be observed that the experimental results have a maximum deviation of 200 V from the predicted ones. Considering that the HV AC source had a sensitivity of 100 V, a deviation of 200 V between theory and experiments is acceptable. Therefore, the application of the three-leg approach is further validated by this case study of a MV cable.

As a note, the values of E_i in Table 1 coincide because k_s varies from 1.12 10^{-3} to 0.48 10^{-3} when distance BC goes from 10 to 30 mm.

Figure 9. *Tangential electric field profiles for along different path lengths BC of Fig. 8. Position 0 refers to point B, while the triple points placed at 1 cm, 2 cm, and 3 cm correspond to point C*

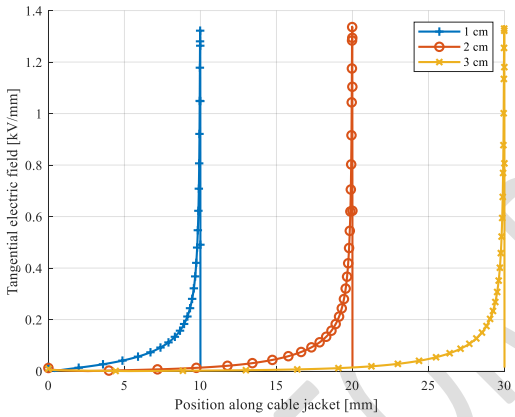

Figure 10. *Example of the PD acquisition and processing with the MV cable (Fig. 8) at 1.1 PDIV, the distance BC being 3 cm. (a) Global cluster and automatic separation map, which highlights two clusters (b) Noise cluster and relevant sub-pattern for the identification (c) PD cluster and relevant sub-pattern for the identification. The PD are identified as 100 % surface discharges*

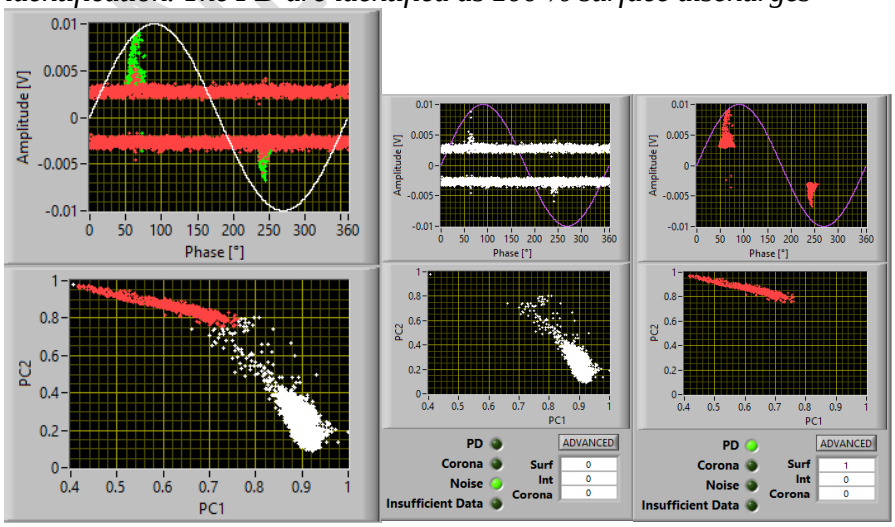

(a) (b) (c)

Table 1. *Maximum field from simulation, E_{sp}, PD inception field from model (2), E_i, estimated PDIV, PDIVe, and measured PDIV, PDIVm, relevant to defective cable model (Fig. 8), at different BC distances*

Distance BC [cm]	E_{sp} [kV/mm]	E_{i} [kV/mm]	$PDIVe$ [kV]	$PDIVm$ [kV]
1	1.32	3.48	2.4	2.63
2	1.34	3.48	2.5	2.60
3	1.34	3.48	2.6	2.60

Effect of Pressure (Altitude) on Surface Insulation Design

The proposed three-leg approach with reliability redundance seems to be the only feasible means to provide specified reliability and safety in electrified transportation, and, even more, in aerospace and for electrical aircrafts. In the latter applications, the further player is the effect of pressure, especially on surface discharges (the slow diffusion dynamics may not change substantially pressure inside bulk cavities or delamination, depending on location of the defect, materials and time at low pressure).

An experiment was devised to investigate the effect of pressure (lower-than - atmospheric) on surface PD inception field (eq. (2)) and PDIV (2nd leg) and PD measurement and phenomenology (3rd leg). A test cell as that in Fig. 11 was built, which can trigger surface discharges and cause accelerated insulation surface aging. The electric field profile for orthogonal and tangential fields are depicted in Fig. 11 b. The latter is able to trigger surface discharges above 0.6 kV at atmospheric pressure, which is both the results obtained from simulation and the measured mean PDIV. Hence, PD test at variable pressure could be carried out above PDIV at each level of pressure.

The test procedure was, in summary:

1. An insulation layer was placed between the electrodes of Fig. 11, with the sample completely flat across the entire face of the electrode.
2. The test cell was placed inside a pressure chamber able to provide values of pressure as low as 10 mbar, in a relative humidity range from 25% to 95%, temperatures from -20°C to 100°C, HV up to 50 kV.
3. Sensor for PD detection was a high frequency current transformer (HFCT), connected to the ground lead of the cell.
4. PDIV was measured on an unaged specimen, at atmospheric pressure, then the pressure was progressively decreased down to 100 mbar. PDIV and PDEV (partial discharge extinction voltage) were measured at various pressure levels, and PD acquired at 1.1 PDIV. Voltage was brought to zero after each PDIV and PDEV measurement, to minimize the specimen surface aging. Testing temperature was 25°C and relative humidity, near to zero.

Figure 12 reports the dependence of PDIV with pressure for a specimen made by Alumina, fitted to the model (2) with k_s calculated according to eq. (3) and the

tangential field profile of Fig. 11 (b). As can be seen, fitting of experimental results to the model is good, thus it seems that the dependence of PDIV and PD inception field with pressure can be reasonably well predicted, at least for pressures lower than standard atmospheric pressure.

Figure 13 shows PRPD pattern, sub-patterns and identification, as in Fig. 10, for measurements performed on Alumina at standard atmospheric pressure and at 50 mbar. It can be observed that identification is still valid, i.e. PD are originated mostly by surface discharges (likelihood of surface discharge goes from 100% at 1000 bar to 76% at 50 mbar). This would support the robustness of the identification algorithm also at low pressure. Last note: PD magnitude is increasing significantly at lower pressure, as also mentioned in [Rui et al. 2010] (but differently from [Lusuardi et al. 2019]).

Figure 11. *(a) Test Set up for surface discharge tests; (b) tangential and orthogonal electric field profiles on the upper specimen side at 1kV.*

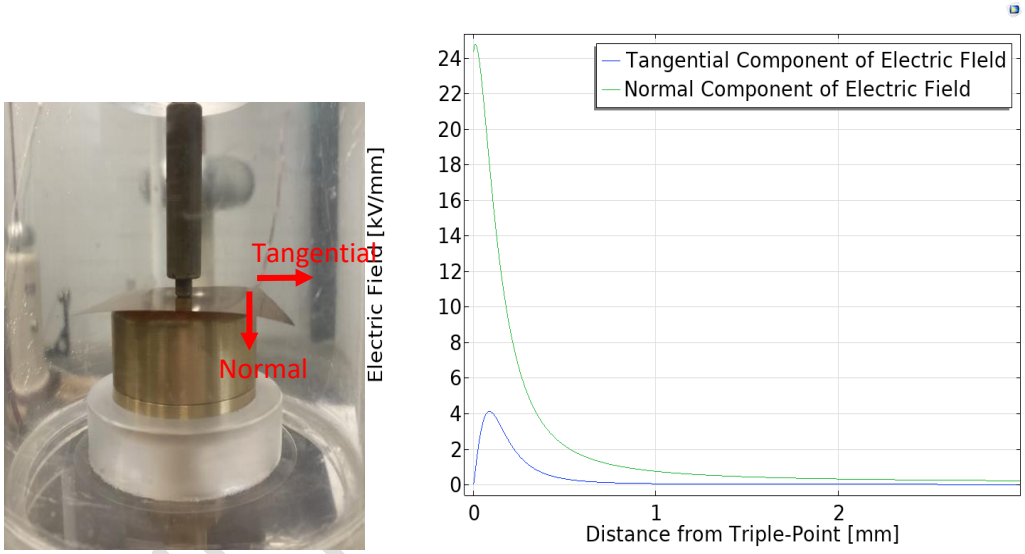

(a) (b)

Figure 12. *Dependence of measured surface PDIV with pressure (down to 50 mbar), fitted to model (2).*

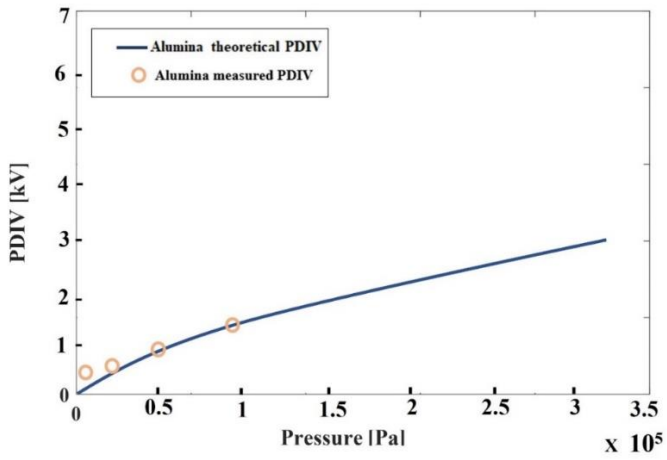

Figure 13. *(a) Phase-resolved PD (PRPD) pattern (b) Example PD pulse (c) global pattern and Separation (PCA) map (d) Sub-maps and sub-patterns (e) Identification for Alumina at 1 bar*

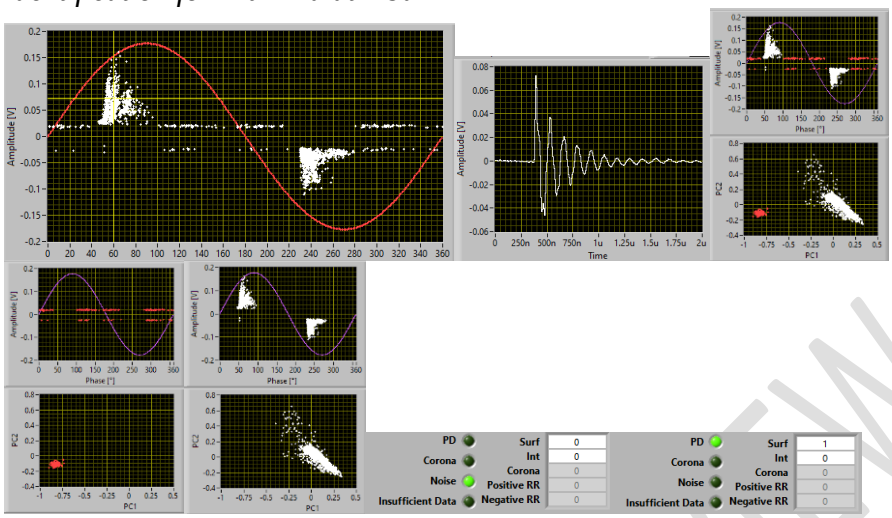

Figure 14. *a) Phase-resolved PD (PRPD) pattern (b) Example PD pulse (c) global pattern and Separation (PCA) map (d) Sub-maps and sub-patterns (e) Identification for Alumina, at 50 mbar*

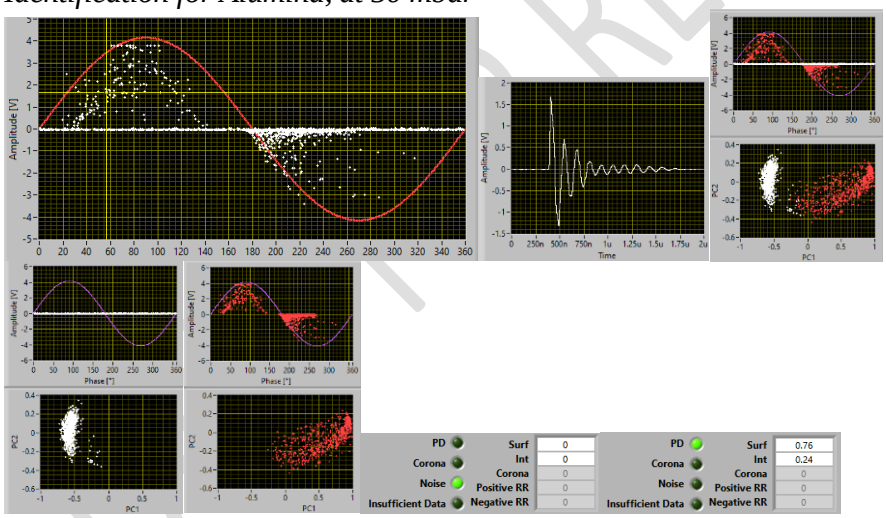

Conclusions

Innovation in insulation system design for electrified transportation and, in general, for critical electrical assets, is needed in order to achieve and preserve reliability and resilience which may be at risk compared to conventional electrical assets (as, e.g., electrical distribution networks).

The approach illustrated in this paper can be a valid strategy for such a purpose: design can be PD free, which, considering that PD are the major cause of breakdown of electrical insulation systems, should guarantee the specified life (once design stresses have been defined and aging modelled properly). On the

other hand, manufacturing, commissioning and unpredictable aging rate magnitude may grow insulation defects that can incept the PD during service. The consequent risk of premature failure can be mitigated by a reliability redundancy concept, e.g., by the use of materials that have been designed to have enhanced endurance to PD. This approach can be effective also when constraints, as volume, specific power, temperature, cannot allow a PD-free design to be achieved, at least in some conditions as under reduced pressure, and when aging effect cannot be predicted and controlled.

This may start a new era in insulation system design for electrified transportation (and not only), where the knowledge of the physics behind degradation phenomena and the availability of enhanced stress modelling tools could replace the main drivers to insulation system design used until now, from on-field experience to macroscopic parameters as creepage and clearance. The objective is to avoid possibly sources of extrinsic aging in an insulation system and, in case, having used materials that can withstand such extrinsic stresses till the specified life.

References

Cambareri, P., & Montanari G.C. (2022) Derivation of a Surface Discharge Model for the Design of the Surface Components of Insulation Systems used in Industrial Electronics Environment, *IEEE Journal of Emerging and Selected Topics in Industrial Electronics*, JESTIE, pp. 1-8.

Contin, A., Cavallini, A., Montanari, G. C., Pasini, G., & Puletti, F. (2002). Digital detection and fuzzy classification of partial discharge signals. *IEEE Transactions on dielectrics and electrical insulation*, 9(3), 335-348.

Lusuardi, L., Rumi, A., Neretti, G., Seri, P., & Cavallini, A. (2019). Assessing the severity of partial discharges in aerospace applications. In *IEEE Conference on Electrical Insulation and Dielectric Phenomena (CEIDP)*, pp. 267-270.

Montanari, G.C., Morshuis, P., Seri, P., & Ghosh, R. (2020). Ageing and reliability of electrical insulation: The risk of hybrid AC/DC grids. *High Voltage*, 5(5), 620-627.

Montanari, G. C., Hebner, R., Morshuis, P., & Seri, P. (2019a). An approach to insulation condition monitoring and life assessment in emerging electrical environments. *IEEE Transactions on Power Delivery*, 34(4), pp.1357-1364.

Montanari, G.C., Yang, Q., Nath D., & Cambarieri P., (2022a). On the design of the surface subsystems of insulators for HV and MV apparatus under AC voltage, *submitted to IEEE Trans. on Power Delivery*.

Montanari, G.C. (2019b). The potential impact of flexible DC transmission and distribution on insulated cables: Accelerated aging and premature failure. *In IEEE PES Asia-Pacific Power and Energy Engineering Conference*, pp. 1-4.

Montanari, G. C., Schwartz, S., Yang, Q., Nath, D., Ghosh, R., & Cuzner, R. (2022a). Towards Partial Discharge Automatic and Unsupervised Monitoring: A Technological Breakthrough for MV Electrical Asset Condition Monitoring and Diagnostics. *In 9th International Conference on Condition Monitoring and Diagnosis (CMD)*, pp. 588-592.

Nath, D., Yang, Q., Montanari, G.C., Yin, W., Xiong, H., & Younsi, K. (2023). Modeling and Characterization of Surface Discharges in Insulating Material for Spacers:

Electrode Shape, Discharge Mode, and Revision of the Creepage Concept. *Materials*, 16(3), 989.

Niemeyer, L. (1995) A generalized approach to partial discharge modelling. *IEEE Trans. Dielectr. Electr. Insul.*, , 2(4), pp. 510-528.

Ramin, R., Montanari, G. C., & Yang, Q. (2021). Designing the Insulation System for Motors in Electrified Aircraft: Optimization, Partial Discharge Issues and Use of Advanced Materials. *Materials*, 14(24), 7555.

Rui, R., & Cotton, I. (2010). Impact of low pressure aerospace environment on machine winding insulation. *In IEEE International Symposium on Electrical Insulation*, pp. 1-5.

Yang, Q., Ghosh, R., & Montanari, G.C. (2023) Tools for partial discharge and health condition inference in aircraft and aerospace electrical asset components", *IEEE EATS*, San Diego, USA, pp. 1-5.

Yang, Q., Montanari G. C., & Nath D. (2023) A global approach to the design of insulation systems for aerospace electrical assets: focus on Printed Circuit Board. *IEEE Trans. on Aerospace and Electronics Systems*, pp. 1-10.